Use of poly-cation oxides to lower the temperature of two-step thermochemical water splitting

Journal:	*Energy & Environmental Science*
Manuscript ID	EE-ART-01-2018-000050.R1
Article Type:	Paper
Date Submitted by the Author:	09-May-2018
Complete List of Authors:	Zhai, Shang; Stanford University, Mechanical Engineering Rojas, Jimmy; Stanford University, Mechanical Engineering Ahlborg, Nadia; Stanford University, Materials Science & Engineering Lim, Kipil; Stanford Synchrotron Radiation Lightsource, Materials Science Toney, Michael; Stanford Synchrotron Radiation Laboratory, Jin, Hyungyu; Pohang University of Science and Technology, Mechanical Engineering Chueh, William; California Institute of Technology, Materials Science Majumdar, Arunava; Stanford University

Use of poly-cation oxides to lower the temperature of two-step thermochemical water splitting

Shang Zhai[a], Jimmy Rojas[a], Nadia Ahlborg[b], Kipil Lim[b,c], Michael F. Toney[c], Hyungyu Jin[a,f,*], William C. Chueh[b,d,e,*], Arun Majumdar[a,d,*]

[a] Department of Mechanical Engineering, Stanford University, Stanford, CA 94305, USA.

[b] Department of Materials Science and Engineering, Stanford University, Stanford, CA 94305, USA.

[c] Stanford Synchrotron Radiation Lightsource, SLAC National Accelerator Laboratory, Menlo Park, CA 94025, USA.

[d] Precourt Institute for Energy, Stanford University, Stanford, CA 94305, USA.

[e] Stanford Institute of Materials and Energy Sciences, SLAC National Accelerator Laboratory, Menlo Park, CA 94025, USA.

[f] Department of Mechanical Engineering, Pohang University of Science and Technology (POSTECH), Pohang 37673, South Korea.

[*] Corresponding authors:
hgjin@postech.ac.kr; wchueh@stanford.edu; amajumdar@stanford.edu

Abstract

We report the discovery of a new class of oxides – poly-cation oxides (PCOs) – that consists of multiple cations and can thermochemically split water in a two-step cycle to produce hydrogen (H_2) and oxygen (O_2). Specifically, we demonstrate H_2 yields of 10.1 ± 0.5 mL-H_2/g and 1.4 ± 0.5 mL-H_2/g from $(FeMgCoNi)O_x$ ($x \approx 1.2$) with thermal reduction temperatures 1300°C and 1100°C, respectively, and also with background H_2 during water splitting step. Remarkably, these capacities are mostly higher than those from measurements and thermodynamic analysis of state-of-the-art materials such as (substituted) ceria and spinel ferrites. Such high-performance two-step cycles within 1100°C are practically relevant for today's chemical infrastructure at large scales, which relies almost exclusively on thermochemical transformations in this temperature regime. It is likely that PCOs with complex cation compositions will offer new opportunities for both fundamental investigations in redox thermochemistry as well as scalable H_2 production using infrastructure-compatible chemical systems.

Broader context

The ability to split water to produce hydrogen is vitally important in energy sciences, with potential broad impact to help decarbonize the global energy system. To achieve this goal, one would require hydrogen from water splitting at the Gigatonne scale, i.e. at the same order of magnitude as CO_2 emissions. Today's chemical infrastructure at the Gigatonne scale relies almost exclusively on *thermochemical transformations* at temperatures ≤ 1100°C. Yet, there are no viable materials that can thermochemically split water in a relatively simple two-step cycle and produce appreciable hydrogen yields in this temperature regime at non-negligible H_2O-to-H_2 conversions. We report here the discovery of a new class of materials – poly-cation oxides (PCOs) – that can split water to produce hydrogen at temperatures as low as 1100°C in a two-step cycle. To date, this has not been shown with state-of-the-art materials such as doped ceria, spinel ferrites, and perovskites, all requiring >1300°C reduction temperatures to yield appreciable hydrogen. PCOs discussed in this work contain four or more cations, and are prevented from phase separating into binary oxides by the entropy of mixing. We propose that this phase stability is responsible for the unusual properties of PCOs for thermochemical water splitting. Our discovery opens a new direction of scientific inquiry in redox thermochemistry as well as the opportunity for scalable hydrogen production.

The ability to split water to produce hydrogen (H_2) is vitally important in energy science[1] with broad applications to store intermittent solar and wind electricity, as a transportation fuel, as a reducing agent to convert carbon dioxide into organics including fuels[2,3], and to decarbonize the existing petrochemical and fertilizer industries[4]. Today's chemical infrastructure at large scales relies almost exclusively on thermochemical transformations at temperatures $\leq$ 1100°C[4,5], which has led to a search for materials and mechanisms for thermochemical water splitting (TWS) below this temperature. Although multi-step thermochemical cycles[5,6] and hybrid cycles[7,8] have made progress in lowering reaction temperatures, their system complexity present challenges for scale up. In that respect, two-step TWS, as shown in **Figure 1**, has received substantial attention due to its relative simplicity[9–22]. In two-step TWS, a metal oxide (MO_x) undergoes a redox cycle, first releasing oxygen (O_2) [$MO_x \rightarrow MO_z + (x - z)/2\ O_2$] during thermal reduction at high temperature, T_H, and at a specific O_2 partial pressure ($p(O_2)$). When subsequently exposed to water vapor at a lower temperature, T_L, it enables water splitting and returns to MO_x [$MO_z + (x - z)H_2O \rightarrow MO_x + (x - z)H_2$]. The thermodynamic cycle is essentially a redox heat engine.

The state-of-the-art materials such as (substituted) ceria and spinel ferrites (specifically for MFe_2O_4 in this paper, where M is Mg, Ni, Co, Fe, etc., or their combinations) require T_H ~1300 to 1500°C[9,11–14,23–28], and they do not produce meaningful amounts of O_2 with $T_H \leq$ 1100°C[19,29]. Many of the perovskites that have been studied can be easily reduced at moderate T_H, but require large amounts of excess steam to produce H_2 during the water-splitting step[15–18,22]; some perovskites[17,30] with good steam-to-H_2 conversion require high T_H similar to ceria and spinel ferrites.

The key requirements and challenges for two-step TWS are threefold: large O_2 release at low $T_H \leq$ 1100°C; high steam-to-H_2 conversion at T_L; and the long-term cyclability of both the reactor and the redox material. A high steam-to-H_2 conversion, in particular, is necessary for good cycle efficiency[18,24,27,31–33]. To lower T_H in two-step TWS while maximizing steam-to-H_2 conversion, thermodynamic analysis[19,29] shows that the partial molar enthalpy and entropy (ΔH_O and ΔS_O, respectively) of the redox oxide must fall within a desirable range. This range, defined by negative Gibbs free energy changes ($\Delta G < 0$) for the two reactions at T_H and T_L, offers a narrow window of thermodynamic feasibility. For (substituted) ceria and spinel ferrites, the ΔH_O and ΔS_O fall in this window when $T_H \geq$ 1400°C and $p(O_2) = 10^{-5}$ atm [19,34–42], resulting in reasonable H_2 yield. While it is possible to reach $T_H \geq$ 1400°C in today's

chemical industry, to do so with cost-effective materials without degradation warrants $T_H \leq$ 1100°C [5]. Moreover, sublimation and loss of the metal oxide is a significant concern[19], even for ceria[43], which is typically regarded as a highly stable material for TWS. For perovskite oxides (e.g., $LaMnO_{3-x}$ family)[16–18,44,45], the relatively small ΔH_O gives rise to large oxygen deficiency at moderate T_H, in contrast to ceria, but their small ΔS_O also means that H_2 generated at T_L will back-react to reduce the perovskite and depress the steam-to-H_2 conversion. These three requirements motivate us to search for materials that could evolve O_2 at a lower T_H and split water in the presence of background H_2.

Rost et al. recently discovered a new class of oxides – entropy stabilized oxides (ESOs) – that exchange oxygen via a reversible solid-solid phase transition[46]. They mixed equimolar quantities of multiple metal oxides (MgO, CoO, NiO, CuO and ZnO) of various crystal structures and heated them up to 1000°C in air; the entropy of mixing of the large number of cations stabilizes the complex oxide denoted as (MgCoNiCuZn)O within only one rocksalt structure, during which the oxide loses some O_2 to the environment. At lower temperatures, this ESO undergoes phase separation into rocksalt and tenorite structures also by entropic driving force. Meanwhile, O_2 is absorbed from the environment.

Inspired by ESOs, here we expand the idea of cation mixing to a broader class of materials, poly-cation oxides (PCOs), and demonstrate two-step TWS. A PCO has three or more metal cations distributed between two different solid phases (e.g., rocksalt and spinel) whose ratio can swing during oxygen exchange, such as two-step TWS between T_H and T_L. Unlike ESOs, however, PCOs need not undergo a complete transition to a single phase, but instead contain a mixture of phases whose fractions swing between T_H and T_L. We demonstrate that the PCO $(FeMgCoNi)O_x$ can split water with $T_H \leq$ 1100°C and with a reasonable tolerance for H_2 oxidation back-reaction at T_L, a prerequisite towards achieving a substantial steam-to-H_2 conversion in a technologically-relevant reactor.

The PCOs and spinel ferrites were synthesized using sol-gel (SG) and solid-state (SS) techniques. SG synthesis allowed us to produce particles with a small grain size of ~0.5 μm (**Figure S1a**); slight sintering was observed after two cycles at T_H = 1300°C (**Figure S1d**). SS synthesis requires a 4-hour calcination step at 1350°C and produces particles with >~10 μm diameter (**Figure S1f**) agglomerated into millimeter-sized pieces. The two-step TWS experiments were performed using a thermogravimetric analyzer (TGA) connected to a gas

chromatograph (GC) and then an O_2 sensor, as shown in **Figure S2**. Because the reaction rate in the TGA can be limited by the temperature ramp rate and the gas flow rate and dynamics, a stagnation flow reactor with a mass spectrometer (**Figure S4a**) was used to measure kinetics. Synthesis and experimental methods are detailed in **Electronic Supplementary Information (ESI)**.

First, we employed TGA-GC to characterize the H_2 productivity of $(FeMgCoNi)O_x$ at different combinations of T_H and T_L, and compared the performance to the well-studied materials CeO_2 and spinel ferrites $NiFe_2O_4$ and $CoFe_2O_4$. **Figures 2a-b** include the H_2 yields of different materials under the following temperature conditions: (1) T_H = 1300°C and T_L = 800°C; (2) T_H = 1100°C and T_L = 800°C. In both cases, thermal reduction (TR) was performed for 5 hours (hrs) at T_H, and water splitting (WS) was performed for 5 hrs at T_L. To first demonstrate thermodynamic feasibility, the long cycle time was chosen to allow the material to approach the thermodynamic equilibrium with the purge gas. During the TR step, Ar was flowed to maintain background $p(O_2)$ ~10 ppm (5 to 15 ppm). During the WS step at condition (1), 91 ppm H_2 and 9.47% H_2O (equivalently, $p(H_2):p(H_2O)$ = 1:1045, abbreviated as $H_2:H_2O$ below) in balance with Ar was used as background; whereas at condition (2), 4.5 ppm H_2 and 9.47% H_2O (equivalently, $H_2:H_2O = 1 : 2.1\times10^4$) balanced with Ar was used. Such H_2 background simulates the case of a batch reactor system, in which product H_2 is not quickly swept away and allowed to back-react with oxide sample; the background $H_2:H_2O$ also indicates steam-to-H_2 conversion (see later experiments with various $H_2:H_2O$ ratios). The H_2 yields for CeO_2 are for the thermodynamic limit of H_2 production (indicated by *) derived from literature[34,42] (details of calculation in **ESI**).

Assuming full redox conversion between Fe^{2+} and Fe^{3+}, the H_2 production capacity of Fe-based oxides would correspond to 0.5 mol of H_2 per 1 mol of Fe. We call such capacity the "redox limit". Nickel ferrite ($NiFe_2O_4$), for example, has a redox limit of 95.6 mL-H_2/g, an order of magnitude higher than the experimental yields. The redox limit of $(FeMgCoNi)O_x$ ($x \approx 1.2$) is estimated to be 40.7 mL-H_2/g. The x value was determined assuming Fe is +3, Co is a mixture of +2 and +3 (the same as in Co_3O_4), and Mg and Ni are +2, according to the X-ray absorption near-edge structure (XANES) discussed later.

As shown in **Figure 2a**, at T_H = 1300°C and T_L = 800°C and $H_2:H_2O$ = 1:1045, the PCO

(FeMgCoNi)O_x yields 10.1 ± 0.5 mL-H_2/g, which is 24.8% ("normalized yield") of its redox limit. The normalized yield of the (FeMgCoNi)O_x is more than three times that of the spinel ferrites. In **Figure 2b**, at T_H = 1100°C and T_L = 800°C and H_2:H_2O = 1 : 2.1×10^4, the (FeMgCoNi)O_x shows the normalized yield more than ten times that of the spinel ferrites. These H_2 yields are higher than those from CeO_2 and spinel ferrites, and the difference is especially striking for the cycles involving T_H = 1100°C and T_L = 800°C when (FeMgCoNi)O_x shows > 5 times higher H_2 producing capacity.

Thermodynamic equilibrium calculations (details in **ESI**) predict that reduction of $NiFe_2O_4$ to $NiFe_2O_{3.87}$ at T_H = 1300°C and $pO_2 = 10^{-5}$ atm will subsequently give a H_2 yield of 9.5 mL/g when WS occurs at T_L = 800°C and H_2:H_2O = 10^{-3}, resulting in $NiFe_2O_{3.97}$ (and 10.0 mL-H_2/g for $CoFe_2O_4$, between $CoFe_2O_{3.87}$ and $CoFe_2O_{3.975}$). For T_H = 1100°C and T_L = 800°C and H_2:H_2O = 1 : 2.1×10^4, the thermodynamic equilibrium limit for $NiFe_2O_4$ is 2.9 mL-H_2/g and 0.2 mL-H_2/g for $CoFe_2O_4$. The measured H_2 yields from the long cycles of both spinel ferrites are mostly lower than their thermodynamic limits probably due to kinetics limitation and/or background O_2 effects during the WS step (discussed in the TGA-GC part in **ESI**). The measured H_2 yields using (FeMgCoNi)O_x exceed the thermodynamic limits of the spinel ferrites under T_H = 1300°C and T_L = 800°C. These comparisons based on redox and thermodynamic limits suggest that the reactivity of Fe for TWS is significantly enhanced in the PCO compared to the well-studied spinel ferrites (Fe is the only redox active element in the PCO as the following XANES study shows).

We have also used TGA-GC to explore the dependence of H_2 production on the background H_2:H_2O ratio during the WS step. Both TR and WS steps were performed for 5 hours to allow the material to approach the thermodynamic equilibrium with purge gas. **Figure 2c** shows the H_2 yield of SG-synthesized (FeMgCoNi)O_x at T_H = 1300°C and T_L = 800°C and at various background H_2:H_2O ratios. It is compared to the measured yields of SG-synthesized spinel ferrites, and the thermodynamic equilibrium limits of ceria[34,42] and perovskite $La_{0.6}Sr_{0.4}MnO_{3-\delta}$ (LSM40)[18,33,47] (thermodynamic limit calculation methods and results including those for other perovskites are in **ESI**). The PCO (FeMgCoNi)O_x generally produces more H_2 than the spinel ferrites. The perovskites LSM40 as well as LSM20 and LSM30 (both not shown in **Figures 2c-d**) produce less H_2 than (FeMgCoNi)O_x under all the conditions considered[18,48]; the H_2 production of LSMs decays quickly to zero as H_2:H_2O increases to around 1:300. On the other hand, (FeMgCoNi)O_x and spinel ferrites display

better tolerance to reverse reaction with increased H_2:H_2O. CeO_2 is only weakly affected by H_2:H_2O, and its H_2 yield is more heavily affected by the very small extent of reduction at 1300°C and 1100°C. We note some prior work that reported two-step TWS did not use a background H_2 and relied on a large flow rate of water vapor to suppress the reverse reaction, which operates in the regime of vanishing H_2:H_2O ratio[15,22,49,50]. **Figure 2d** shows the same trend at the cycle condition T_H = 1100°C and T_L = 800°C, where (FeMgCoNi)O_x demonstrates an even bigger advantage, albeit the H_2 productivity declines to zero at H_2:H_2O > 1:2009 To summarize, the PCO (FeMgCoNi)O_x produces H_2 at lower temperatures than CeO_2 or spinel ferrites, and demonstrates more resistance to H_2 oxidation reverse reaction during WS than Mn-based perovskites, which has practical significance in scale-up.

Next, to study the kinetics, we have obtained preliminary results of reaction rate by conducting experiments on TWS cycles with TR of 30 min and WS of 1 hr and using TGA-GC to measure H_2 yields. As **Figures 3a-b** shows, at T_H = 1300°C, T_L = 800°C and H_2:H_2O = 1:1045, the H_2 yield of (FeMgCoNi)O_x is about two times higher than that of spinel ferrites and the thermodynamic equilibrium limit for CeO_2; at T_H = 1100°C, T_L = 800°C and H_2:H_2O = 1 : 2.1×10^4, cobalt ferrite produces no H_2, while (FeMgCoNi)O_x still produces appreciable H_2, about two times the yields from nickel ferrite and CeO_2. Additionally, we investigated the cyclability of the PCO. **Figure 3c** shows that the SG-synthesized (FeMgCoNi)O_x in TGA shows almost no performance degradation during the 10 cycles at both temperature conditions. **Figure S5** also demonstrates good cyclability of the SS-synthesized (FeMgCoNi)O_x in the stagnation flow reactor. **Figures S1b-e** show that PCO particles grew to about 1~2 μm after two cycles and keep the similar morphology until after the 10th cycle. For a thorough cyclability investigation for practical applications at least hundreds of cycles are required, which will be the topic of a later study. All of the H_2 yield data in **Figure 3** were taken from the second cycle to eliminate possible randomness in the first one, if not otherwise specified.

Short TWS cycles using PCO were also carried out in the stagnation flow reactor to assess material kinetics (**Figures 3d**, **S4** and **S5**). The H_2 yield from the SS-synthesized (FeMgCoNi)O_x is about 5 mL/g on average, higher than that (~ 3mL/g) from the TGA-GC measurements on the SG-synthesized sample. Considering that the SG-synthesized sample is generally expected to possess better kinetics due to its small particle size and large surface area, this result indicates that good gas transport in stagnation flow reactor largely improves

reaction kinetics. The O_2 release at T_H = 1300°C is significantly faster than the H_2 production at T_L = 800°C and H_2:H_2O = 1:1000. The peak rates of 0.7 mL-O_2/min/g and 0.6 mL-H_2/min/g for (FeMgCoNi)O_x are promising, considering that the SS-synthesized sample consists of ~10 μm particles. The relatively slow water oxidation kinetics is the rate-limiting reaction in the cycle, which deserves further study. The potential elevation of the H_2 signal background due to water fragmentation in the mass spectrometer was accounted for in quantifying the H_2 production from water splitting.

In order to elucidate the redox reaction mechanism of (FeMgCoNi)O_x during two-step TWS, quenching experiments were performed as described in **ESI**, assuming sample structure and properties are maintained when quenched at the end of TR or WS reaction. Such an assumption would be relaxed by in situ experiments. The X-ray diffraction (XRD) results in **Figure 4a** on the quenched (FeMgCoNi)O_x samples confirm that both rocksalt and spinel phases co-exist during thermal cycling, but their ratio changes as temperatures and gas environments vary. We used Rietveld refinement to quantify the fraction of each phase. Since Fe, Co and Ni have very similar atomic scattering factors for X-rays[51], we replaced all the transition metals with Fe in our model. The rocksalt phase was assumed to be Fe_tO ($t \leq 1$) and the spinel phase was assumed to be Fe_3O_4 (reasoning and details in **ESI**). **Figure 4b** shows the volumetric percentage of the rocksalt phase obtained from the Rietveld refinement from three repetitions of (FeMgCoNi)O_x synthesis and quenching (from T_H = 1300°C, T_H = 1100°C and T_L = 800°C). All sets of data show a consistent trend: the phase ratio depends strongly on temperature, and higher temperatures generally produce larger fraction of the rocksalt phase associated with greater O_2 release. Although a phase change is clearly correlated with oxygen exchange, the exact redox mechanism cannot be determined from XRD alone and deserves further study.

We employed XANES to determine which transition metal(s) in the PCO (FeMgCoNi)O_x undergoes an oxidation state change during two-step TWS (it was assumed that Mg does not change its oxidation state). **Figure 4c** shows the XANES spectra of the Fe-edge in (FeMgCoNi)O_x. We compared the energy at the half of the maximum intensity in each of the normalized absorption spectra. The experiments showed that Fe has an edge shift of about 0.6 eV between the WS and TR steps (compares to 4.3 eV between Fe^{2+} and Fe^{3+}), which indicates an oxidation state change of 0.14. XANES plots of Co and Ni are in **Figure S7**. Interestingly, as **Figure 4d** shows, Co and Ni are essentially redox inactive compared to Fe,

suggesting that Fe is the only redox-active element in $(FeMgCoNi)O_x$.

In conclusion, we report a new class of material, poly-cation oxide (PCO), which can thermochemically split water to produce H_2 with remarkably high yields within 1100°C. Particularly, the water splitting performance of PCO $(FeMgCoNi)O_x$ at specific conditions exceeds the thermodynamic limits of state-of-the-art materials such as spinel ferrites, ceria and several LSM perovskites, under specific background H_2:H_2O values during water splitting step. X-ray absorption studies suggest that Fe is the only redox-active species in $(FeMgCoNi)O_x$, which also contain Mg, Ni and Co cations. This raises the intriguing questions about the roles of Mg, Ni and Co in enabling Fe this unprecedented performance to split water at lower temperatures. Fe in well-studied spinel ferrites is purely Fe^{3+} and has been traditionally thought to have bigger redox capacity than a spinel-rocksalt two-phase oxide system (like in PCOs) where both Fe^{2+} and Fe^{3+} are present. Therefore, what remains intriguing is why in such a two-phase system with multiple cations, the redox extent of Fe in $(FeMgCoNi)O_x$ has been significantly improved. A deeper understanding warrants the measurement and modeling of the phase diagram of the PCOs, though we realize the complexity of such an investigation, even for the Fe-Co-O system[52]. Preliminary reaction kinetics data show the slow water splitting kinetics of PCO, suggesting the potential improvement in its kinetics by, for example, reducing PCO particle sizes, adding high melting point support material, and reactor optimization. From the viewpoint of chemical reactor systems, we note that while most reactor architectures for such reactions so far have used solar concentrators as a heat source[10,11,13,19,21,53–56], the increasing availability of low-cost carbon-free electricity[4,57–60] suggests that localized electrical heating could be used for TWS as well, thus opening more options for system architectures using PCOs as the water splitting materials in various configurations.

Conflicts of interest

The authors declare no competing financial interests.

Author Contributions

H.J. and S.Z. conceived the idea of using poly-cation oxides for thermochemical water splitting. A.M., W.C. H.J. and M.T. supervised the work. S.Z., H.J. and J.R. designed various ferrites and synthesized the samples. S.Z., J.R. and N.A. conducted water splitting experiments in TGA-GC; N.A., S.Z., H.J. and J.R. conducted water splitting experiments in stagnation flow reactor. S.Z. and H.J. conducted XRD experiments. S.Z. performed Rietveld refinement analysis and SEM characterization. S.Z., J.R., H.J., and N.A. conducted quenching experiments. K.L. conducted XANES characterization and analysis. S.Z. and N.A. conducted thermodynamic H_2 yield calculations of ceria and LSM perovskites. All authors contributed to writing the manuscript.

Acknowledgements

We would like to thank Po-Chun Hsu and Raghubir Gupta for their help in this work. This work was funded by the Department of Energy, Laboratory Directed Research and Development program at SLAC National Accelerator Laboratory, under contract DE-AC02-76SF00515. Additional support was provided by Stanford (SUNCAT Center), by the Fuel Cell Technology Program in the Office of Energy Efficiency and Renewable Energy of the US Department of Energy and by the Office of Naval Research under grant N00014-17-1-2918. Use of the Stanford Synchrotron Radiation Lightsource, SLAC National Accelerator Laboratory, is supported by the U.S. Department of Energy, Office of Science, Office of Basic Energy Sciences under Contract No. DE-AC02-76SF00515.

References

1 G. W. Crabtree, M. S. Dresselhaus and M. V Buchanan, *Phys. Today*, 2004, **57**, 39–44.

2 G. Centi, E. A. Quadrelli and S. Perathoner, *Energy Environ. Sci.*, 2013, **6**, 1711.

3 C. Ampelli, S. Perathoner and G. Centi, *Philos. Trans. R. Soc. A Math. Phys. Eng. Sci.*, 2015, **373**, 20140177–20140177.

4 M. Benson, S.M., Bras, R., Carter, E., Deutch, J., Majumdar, A., Ort, D., Ramage, M., Socolow, R., Toone, E., Whitesides, G.M., Wrighton, *US Secretary of Energy Advisory Board Report on CO2 Utilization and Negative Emissions Technologies*, 2016.

5 B. Xu, Y. Bhawe and M. E. Davis, *Proc. Natl. Acad. Sci.*, 2012, **109**, 9260–9264.

6 S. Dey, S. Rajesh and C. N. R. Rao, *J. Mater. Chem. A*, 2016, **4**, 16830–16833.

7 G. F. Naterer, S. Suppiah, L. Stolberg, M. Lewis, M. Ferrandon, Z. Wang, I. Dincer, K. Gabriel, M. A. Rosen, E. Secnik, E. B. Easton, L. Trevani, I. Pioro, P. Tremaine, S. Lvov, J. Jiang, G. Rizvi, B. M. Ikeda, L. Lu, M. Kaye, W. R. Smith, J. Mostaghimi, P. Spekkens, M. Fowler and J. Avsec, *Int. J. Hydrogen Energy*, 2011, **36**, 15486–15501.

8 G. F. Naterer, S. Suppiah, L. Stolberg, M. Lewis, Z. Wang, I. Dincer, M. A. Rosen, K. Gabriel, E. Secnik, E. B. Easton, I. Pioro, S. Lvov, J. Jiang, J. Mostaghimi, B. M. Ikeda, G. Rizvi, L. Lu, A. Odukoya, P. Spekkens, M. Fowler and J. Avsec, *Int. J. Hydrogen Energy*, 2013, **38**, 740–759.

9 A. Steinfeld, *Sol. Energy*, 2005, **78**, 603–615.

10 J. R. Scheffe and A. Steinfeld, *Mater. Today*, 2014, **17**, 341–348.

11 C. Agrafiotis, M. Roeb and C. Sattler, *Renew. Sustain. Energy Rev.*, 2015, **42**, 254–285.

12 C. Jarrett, W. Chueh, C. Yuan, Y. Kawajiri, K. H. Sandhage and A. Henry, *Sol. Energy*, 2016, **123**, 57–73.

13 T. Kodama and N. Gokon, *Chem. Rev.*, 2007, 107, 4048–4077.

14 T. Kodama, Y. Kondoh, R. Yamamoto, H. Andou and N. Satou, *Sol. Energy*, 2005, **78**, 623–631.

15 A. H. McDaniel, E. C. Miller, D. Arifin, A. Ambrosini, E. N. Coker, R. O'Hayre, W.

C. Chueh and J. Tong, *Energy Environ. Sci.*, 2013, **6**, 2424.

16 M. Takacs, M. Hoes, M. Caduff, T. Cooper, J. R. Scheffe and A. Steinfeld, *Acta Mater.*, 2016, **103**, 700–710.

17 M. Ezbiri, M. Takacs, D. Theiler, R. Michalsky and A. Steinfeld, *J. Mater. Chem. A*, 2017, **5**, 4172–4182.

18 A. H. Bork, E. Povoden-Karadeniz and J. L. M. Rupp, *Adv. Energy Mater.*, 2017, **7**, 1601086.

19 J. E. Miller, A. H. McDaniel and M. D. Allendorf, *Adv. Energy Mater.*, 2014, **4**, 1300469.

20 Y. Tamaura, A. Steinfeld, P. Kuhn and K. Ehrensberger, *Energy*, 1995, **20**, 325–330.

21 W. C. Chueh, C. Falter, M. Abbott, D. Scipio, P. Furler, S. M. Haile and A. Steinfeld, *Science*, 2010, **330**, 1797–1801.

22 A. H. Bork, M. Kubicek, M. Struzik and J. L. M. Rupp, *J. Mater. Chem. A*, 2015, **3**, 15546–15557.

23 J. R. Scheffe and A. Steinfeld, *Mater. Today*, 2014, **17**, 341–348.

24 W. C. Chueh and S. M. Haile, *Philos. Trans. A. Math. Phys. Eng. Sci.*, 2010, **368**, 3269–94.

25 M. Inoue, N. Hasegawa, R. Uehara, N. Gokon, H. Kaneko and Y. Tamaura, *Sol. Energy*, 2004, **76**, 309–315.

26 S. S. Naghavi, A. A. Emery, H. A. Hansen, F. Zhou, V. Ozolins and C. Wolverton, *Nat. Commun.*, 2017, **8**, 285.

27 Y. Hao, C. K. Yang and S. M. Haile, *Chem. Mater.*, 2014, **26**, 6073–6082.

28 A. Le Gal and S. Abanades, *J. Phys. Chem. C*, 2012, **116**, 13516–13523.

29 B. Meredig and C. Wolverton, *Phys. Rev. B - Condens. Matter Mater. Phys.*, 2009, **80**, 245119.

30 M. Ezbiri, M. Takacs, B. Stolz, J. Lungthok, A. Steinfeld and R. Michalsky, *J. Mater. Chem. A*, 2017, **5**, 15105–15115.

31 I. Ermanoski, J. E. Miller and M. D. Allendorf, *Phys. Chem. Chem. Phys.*, 2014, **16**, 8418–27.

32 D. R. Barcellos, S. Michael, J. Tong, W. Chueh, A. H. McDaniel and R. P. O'Hayre, 2017, Personal communication.

33 J. R. Scheffe, D. Weibel and A. Steinfeld, *Energy & Fuels*, 2013, **27**, 4250–4257.

34 R. J. Panlener, R. N. Blumenthal and J. E. Garnier, *J. Phys. Chem. Solids*, 1975, **36**, 1213–1222.

35 R. N. Blumenthal and J. E. Garnier, *J. Solid State Chem.*, 1976, **16**, 21–34.

36 G. Zhou and R. J. Gorte, *J. Phys. Chem. B*, 2008, **112**, 9869–9875.

37 D. DJUROVIC, M. ZINKEVICH and F. ALDINGER, *Solid State Ionics*, 2008, **179**, 1902–1911.

38 T. Kobayashi, *Solid State Ionics*, 1999, **126**, 349–357.

39 I.-H. Jung, S. A. Decterov, A. D. Pelton, H.-M. Kim and Y.-B. Kang, *Acta Mater.*, 2004, **52**, 507–519.

40 T. Kim, J. M. Vohs and R. J. Gorte, *Ind. Eng. Chem. Res.*, 2006, **45**, 5561–5565.

41 P. R. Shah, T. Kim, G. Zhou, P. Fornasiero and R. J. Gorte, *Chem. Mater.*, 2006, **18**, 5363–5369.

42 M. Zinkevich, D. Djurovic and F. Aldinger, *Solid State Ionics*, 2006, **177**, 989–1001.

43 N. P. Siegel, T. Garino, E. N. Coker, S. Livers, A. Ambrosini, J. E. Miller, R. B. Diver and M. Bobek, *SolarPaces Conf.*, 2010, 1–11.

44 M. Oishi, K. Yashiro, K. Sato, J. Mizusaki and T. Kawada, *J. Solid State Chem.*, 2008, **181**, 3177–3184.

45 T. Nakamura, K. Yashiro, K. Sato and J. Mizusaki, *Solid State Ionics*, 2009, **180**, 368–376.

46 C. M. Rost, E. Sachet, T. Borman, A. Moballegh, E. C. Dickey, D. Hou, J. L. Jones, S. Curtarolo and J.-P. Maria, *Nat. Commun.*, 2015, **6**, 8485.

47 H. Tagawa, in *Proceedings of the 5th International Symposium on Solid Oxide Fuel Cells (SOFC-V)*, Aachen, Germany, 1997.

48 J. Mizusaki, N. Mori, H. Takai, Y. Yonemura, H. Minamiue, H. Tagawa, M. Dokiya, H. Inaba, K. Naraya, T. Sasamoto and T. Hashimoto, *Solid State Ionics*, 2000, **129**, 163–177.

49 Q. Jiang, Z. Chen, J. Tong, M. Yang, Z. Jiang and C. Li, *ACS Catal.*, 2016, **6**, 1172–1180.

50 P. Singh and M. S. Hegde, *Chem. Mater.*, 2010, **22**, 762–768.

51 D. Carta, M. F. Casula, A. Falqui, D. Loche, G. Mountjoy, C. Sangregorio and A. Corrias, *J. Phys. Chem. C*, 2009, **113**, 8606–8615.

52 I.-H. Jung, S. A. Decterov, A. D. Pelton, H.-M. Kim and Y.-B. Kang, *Acta Mater.*, 2004, **52**, 507–519.

53 R. B. Diver, J. E. Miller, M. D. Allendorf, N. P. Siegel and R. E. Hogan, *J. Sol. Energy Eng.*, 2008, **130**, 41001.

54 C. L. Muhich, B. D. Ehrhart, I. Al-Shankiti, B. J. Ward, C. B. Musgrave and A. W. Weimer, *Wiley Interdiscip. Rev. Energy Environ.*, 2016, 5, 261–287.

55 S. Abanades, P. Charvin, G. Flamant and P. Neveu, *Energy*, 2006, **31**, 2469–2486.

56 A. Steinfeld, *Sol. Energy*, 2005, **78**, 603–615.

57 S. Chu and A. Majumdar, *Nature*, 2012, 488, 294–303.

58 R. Wiser and M. Bolinger, *Renew. Energy*, 2011, **69**, 98.

59 S. Schmela, Michael, B. I. Gaëtan, Masson and B. I. Nhan Ngo Thi Mai, *Sol. Mark. Rep.*, 2016, 60.

60 SolarPower Europe, *Glob. Mark. Outlook*, 2014, 32.

Figures

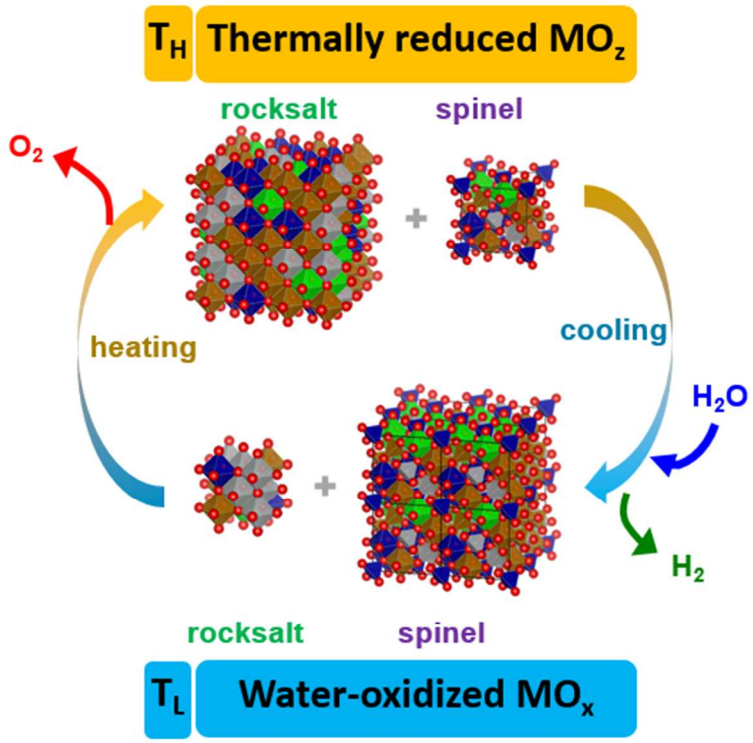

Fig. 1. Schematic of two-step thermochemical water splitting (TWS) using poly-cation oxide (PCO). In a typical two-step TWS, a metal oxide (MO_x) becomes thermally-reduced at a higher temperature, T_H, and releases O_2 to produce MO_z ($z < x$). The reduced oxide is cooled to a lower temperature, T_L, where it is oxidized by water to produce H_2 as it returns to MO_x. In PCOs, a reversible phase swing between rocksalt (reduced) and spinel (oxidized) phases occurs during thermochemical cycling. The rocksalt-to-spinel ratio becomes larger at T_H compared to that at T_L.

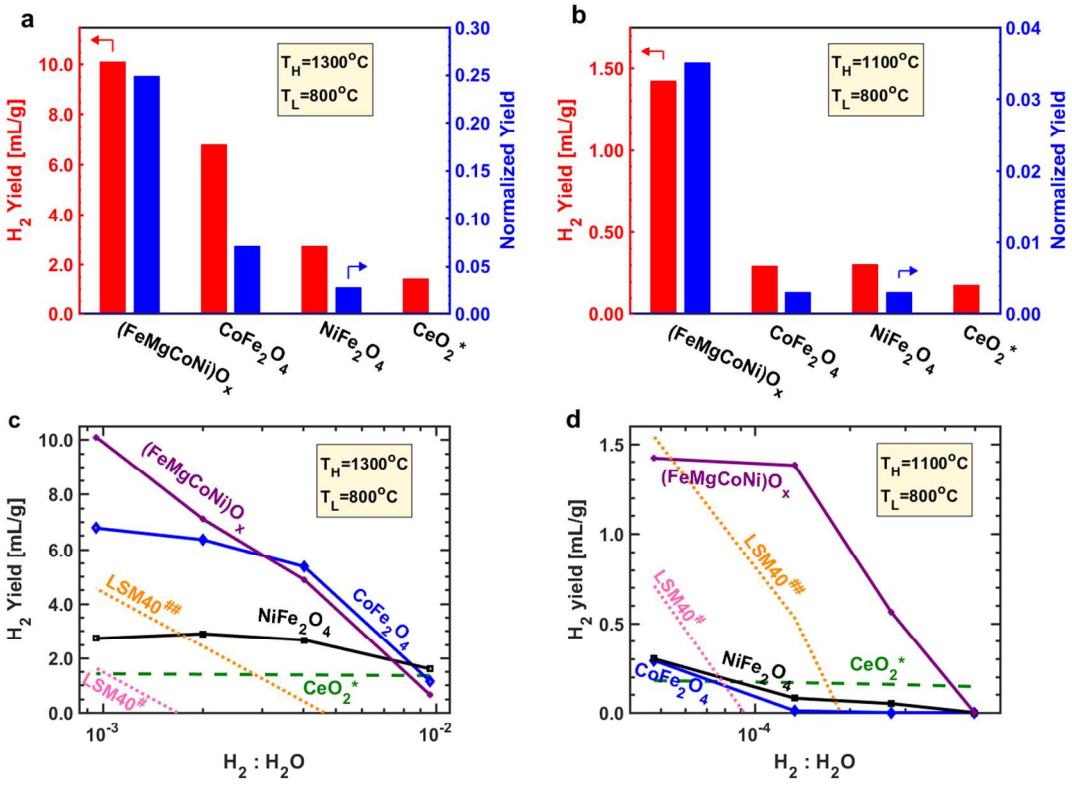

Fig. 2. Thermochemical water splitting performance with various background H_2:H_2O for long cycles. (FeMgCoNi)O_x and spinel ferrites went through thermal reduction at T_H for 5 hours and water splitting at T_L in specific background pH_2:pH_2O for 5 hours. (**a, b**) H_2 yields from long cycle with sol-gel (SG) synthesized samples. The CeO_2 data are from thermodynamic equilibrium limits, see data in **Tables S6 and S7.** "Redox limit" is defined by assuming all Fe atoms go through +2/+3 redox swing. Normalization by such redox limit is indicated as "Normalized Yield". Reaction conditions are (**a**) T_H = 1300°C, T_L = 800°C and H_2:H_2O = 1 : 10^3; (**b**) T_H = 1100°C, T_L = 800°C and H_2:H_2O = 1 : 2.1×10^4. (**c, d**) Influence of H_2:H_2O during water splitting step on performance of SG-synthesized (FeMgCoNi)O_x and spinel ferrites, along with CeO_2, perovskite LSM40 ($La_{0.6}Sr_{0.4}MnO_{3-\delta}$). The H_2 yields of CeO_2 and LSM40 represent calculations of the thermodynamic limit, indicated by *[34,42], #[18] and ##[33,47], whereas the H_2 yields

for $(FeMgCoNi)O_{x,}$ and spinel ferrites where measured; values are in **Table S6** and **Table S7**.

All measurements were conducted with TGA-GC. Background pO_2 is about 10 ppm.

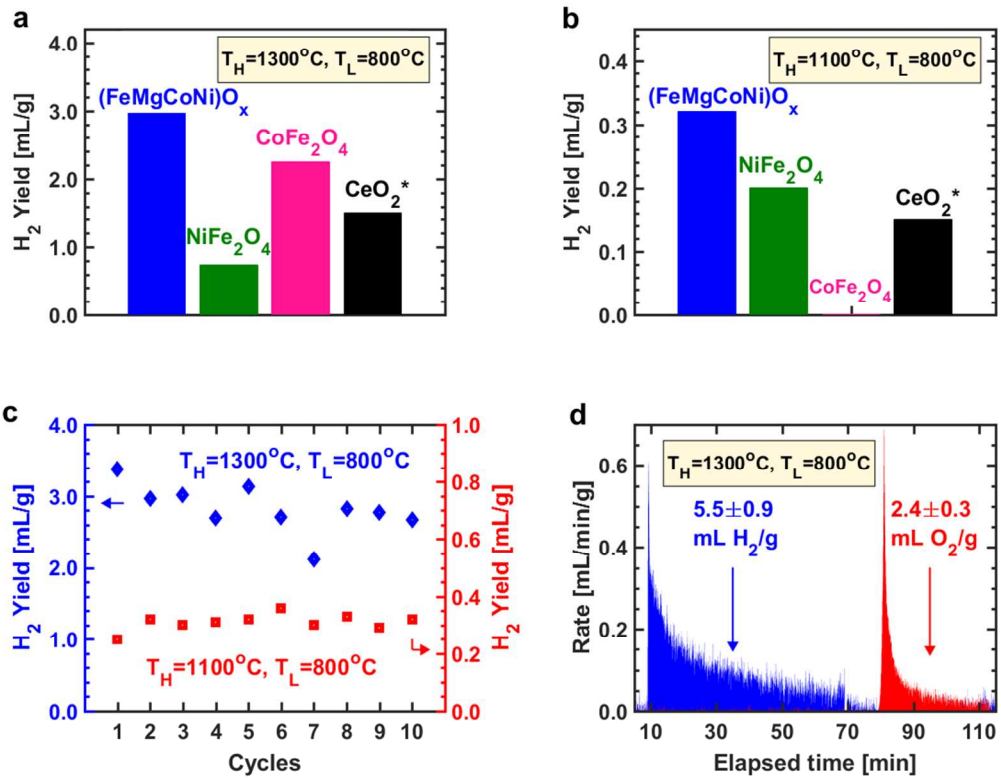

Fig. 3. Thermochemical water splitting performance of for short cycles. (**a**) T_H = 1300°C and $pO_2 = 10^{-5}$ atm, T_L = 800°C and H_2:H_2O = 1 : 10^3, sol-gel (SG) synthesized PCO (FeMgCoNi)O_x and spinel ferrites. (**b**) T_H = 1100°C and $pO_2 = 10^{-5}$ atm, T_L = 800°C and H_2:H_2O = 1 : 2.1×10^4, SG-synthesized (FeMgCoNi)O_x and spinel ferrites. The CeO_2 data are from thermodynamic equilibrium limits. (**c**) 10-cycle measurements using SG-synthesized (FeMgCoNi)O_x under the same conditions as (**a**) and (**b**), respectively. (**d**) Kinetics of a typical cycle in the stagnation flow reactor for solid-state (SS) synthesized (FeMgCoNi)O_x at the same conditions as (**a**). The errors come from background drift of mass spectrometer signals.

All the samples went through "short cycles" with 30 min TR at T_H and 1 hr WS at T_L; the H_2 yields data were taken from the 2nd (short) cycle if not otherwise specified. Except for (**d**), all results were obtained using TGA-GC.

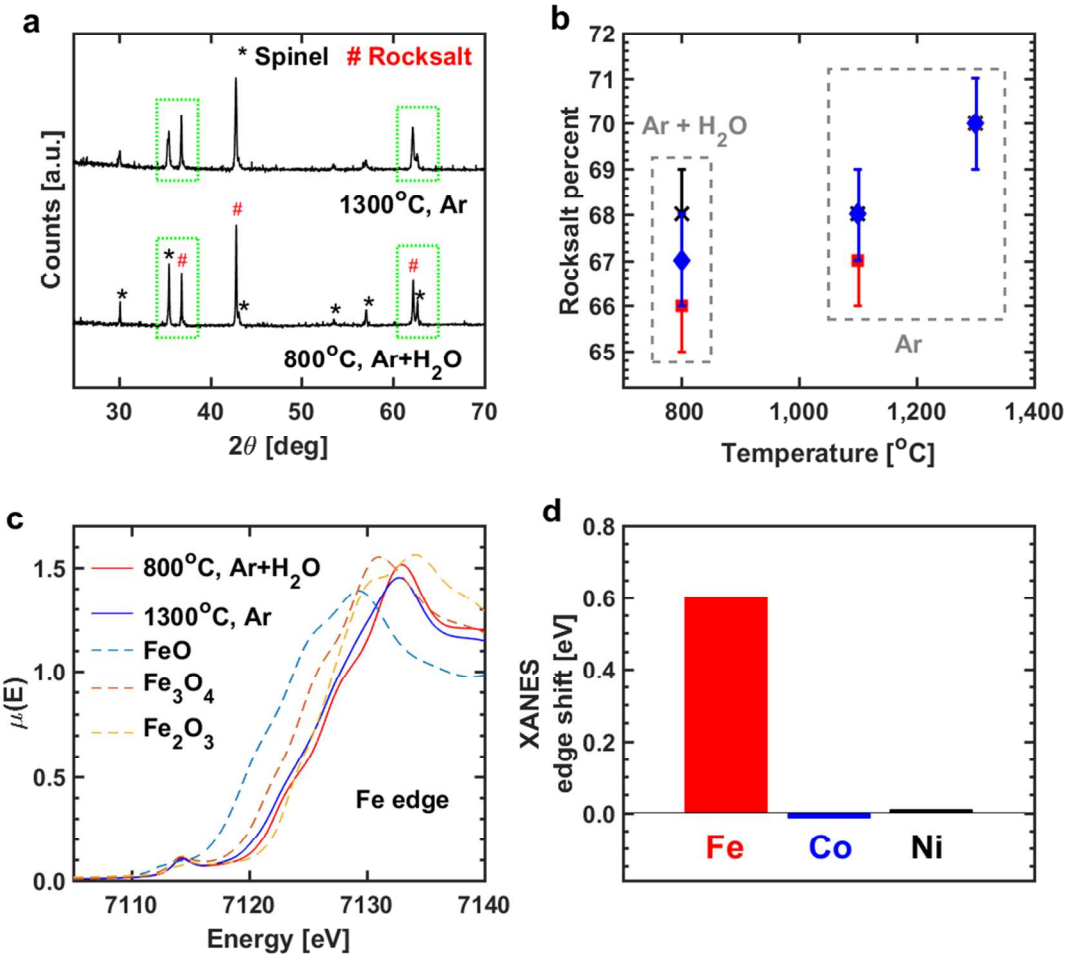

Fig. 4. Structural and elemental characterizations of quenched (FeMgCoNi)O_x. (**a**) Cu Kα X-ray diffraction (XRD) of thermally reduced and water-oxidized (FeMgCoNi)O_x obtained by quenching from each corresponding condition. The quenching conditions are: (1) T_H = 1300°C and $pO_2 = 10^{-5}$ atm for 30 min; (2) T_L = 800°C and 10 vol. % H_2O for 1 hour after thermal reduction at T_H = 1300°C and $pO_2 = 10^{-5}$ atm for 30 min. The change of peak intensity qualitatively illustrates the rocksalt-spinel phase swing in this oxide. (**b**) Rietveld refinement result of XRD patterns at various quenching conditions. Three sets of (FeMgCoNi)O_x were made by solid-state synthesis and quenched separately at three different conditions: (1) and (2) are the same as above; (3) T_H = 1100°C and $pO_2 = 10^{-5}$ atm for 30 min. Refinement results of each set

are shown by one color/shape (blue diamond, red square, and black cross) of symbols with error bars (There are overlaps among error bars.). (**c**) X-ray absorption near edge structure (XANES) result for the Fe edge of the quenched (FeMgCoNi)O_x samples. The dashed lines indicate reference data of different iron oxides. The shift of Fe oxidation state is clearly demonstrated between the oxidized and reduced states. (**d**) Amount of edge shift (eV) for Fe, Co, and Ni between the reduced and oxidized states of (FeMgCoNi)O_x measured by XANES. Fe is the redox-active cation in this PCO.